CrossMark

Influence of SMAT Parameters on Microstructural and Mechanical Properties of Al-Mg-Si Alloy AA 6061

S. Anand Kumar, P. Satish Kumar, S. Ganesh Sundara Raman, and T.S.N. Sankara Narayanan

In the present work, the influence of surface mechanical attrition treatment (SMAT) parameters on the microstructural and mechanical properties of an aluminum-magnesium-silicon alloy AA 6061 was studied using design of experiment technique. Balls of three different diameters were used, and SMAT was done for three different durations. The microstructural features of the surface layer fabricated by SMAT were characterized by cross-sectional scanning electron microscopic observations, x-ray diffraction technique and transmission electron microscopy. The microindentation hardness, nanoindentation hardness and surface roughness were determined. Due to SMAT, nanocrystallites formed on the surface and near-surface regions, and hardness and surface roughness increased. The ball diameter was the most influencing SMAT parameter compared to the treatment duration. However, interaction between ball diameter and treatment duration could not be ignored. Regression equations were developed relating the process parameters to the surface properties. The ball diameter and treatment duration could thus be properly selected as per the required values of roughness and/or the hardness.

1. Introduction

As many failures occur through damaging mechanisms such as fatigue, fretting fatigue, wear and corrosion, which start from the material's surface, enhancing surface properties could combat against these damages (Ref 1). Nanostructured and ultrafine-grained materials exhibit higher yield strength, hardness and enhanced wear resistance compared to their coarse-grained counterparts (Ref 2, 3). Newer advanced processes based on surface severe plastic deformation technique such as air blast shot peening (Ref 4), surface nanocrystallization and hardening (SNH) (Ref 5), ultrasonic shot peening (USSP) (Ref 6, 7) and surface mechanical attrition treatment (SMAT) (Ref 1) have been developed to generate nanocrystalline surface layer.

SMAT is similar to the conventional shot peening to generate a nanocrystallized layer on the surface of metallic materials. It has shown promising results in improving the hardness, fatigue lives and wear resistance of various metallic materials. Chang et al. (Ref 8) have investigated the effect of SMAT on pure aluminum and A356 Al-Si aluminum alloy. They observed a similar mechanism of grain refinement resulting in nanostructured grains

in both materials, such as development of dislocation cells distinguished by dense dislocation walls and dislocation tangles inside the coarse grains or subdivided subgrains. The SMAT-treated A356 Al-Si alloy had thicker nanostructured zone compared to pure aluminum samples. It was attributed to the presence of dispersed fine broken Si particles in SMAT-treated A356 Al-Si alloy, which act as source of dislocation generation.

Owing to their non-equilibrium nature, the nanostructured grains are prone to grow quickly at high temperatures. There are some studies dealing with the thermal stability of nanostructured surface fabricated by SMAT process. Chang et al. (Ref 9) found that nanostructured grains with high-angle grain boundaries exhibited better thermal stability compared to grains separated by low-angle grain boundaries in the submicrometer layer of pure Al and A356 alloy. Liu et al. (Ref 10) investigated the influence of SMAT treatment on the thermal stability and tensile properties of pure aluminum. The yield strength of the SMAT-treated aluminum samples was two times higher compared to untreated aluminum samples. The nanostructured grains of SMAT-treated aluminum samples were stable up to 275 °C.

Wen et al. (Ref 11) observed a thin layer containing iron introduced inside the nanostructured layer of 2024 aluminum alloy due to the material transfer from the steel balls during the SMAT process. The presence of iron-containing layer had degraded the corrosion resistance and enhanced the tribological characteristics of 2024 aluminum alloy. SMAT process has also been employed as a pre-treatment to aluminum and its alloys in order to enhance the properties of coatings. Wen et al. (Ref 12) investigated the corrosion resistance of a composite coating prepared by microarc oxidation technique over SMAT-treated surface of 2024 aluminum alloy. Their results showed an enhancement in the corrosion resistance due to the development of a denser passive film over nanocrystalline surface of 2024 aluminum alloy.

Processing parameters of SMAT play a vital role in successful fabrication of nanostructured surface layer and in realizing desired properties of the materials. In SMAT process, the size of balls employed plays a major role in deciding the

S. Anand Kumar, Department of Mechanical Engineering, School of Engineering, Dayananda Sagar University, Bengaluru, Karnataka, India and Department of Mechanical Engineering, ACS College of Engineering, Bengaluru, Karnataka, India; **P. Satish Kumar,** Quality Assurance Division, Nuclear Fuel Complex, Hyderabad, India; **S. Ganesh Sundara Raman,** Department of Metallurgical and Materials Engineering, IIT Madras, Chennai, India; and **T.S.N. Sankara Narayanan,** Department of Dental Biomaterials, Chonbuk National University, Chonju, South Korea. Contact e-mail: anandkumarait@gmail.com.

microstructural and mechanical properties of the material. The influence of ball size has been studied on the surface hardness, surface roughness and wettability of 316L stainless steel (Ref 13), and fatigue resistance of SMAT-treated 316L stainless steel (Ref 14). Treatment duration is also considered to be one of the key parameters in achieving the desired overall properties. The effect of treatment duration has been studied on the grain size and microstrain of different metallic materials such as 316L stainless steel (Ref 6), pure Fe (Ref 15), low-carbon steel (Ref 16), alpha titanium (Ref 17), on plastic deformation depth (work-hardened layer) of low-carbon steel (Ref 16), 316L stainless steel (Ref 13), pure copper (Ref 18), alpha titanium (Ref 17), Ti-6Al-4V (Ref 19), alloy 718 (Ref 20), wear resistance of pure copper (Ref 21), Ti-6Al-4V (Ref 19), alloy 718 (Ref 20) and fatigue resistance of Ti-6Al-4V (Ref 22), alloy 718 (Ref 23).

In many studies, mechanical properties of SMAT-processed sample have been studied as a function of one SMAT parameter at a time. It is very much necessary to consider the interactions between the SMAT parameters and their overall effects on the properties. The optimized processing conditions to achieve the desired mechanical properties of SMAT-treated metallic materials are very much necessary from the processing and manufacturing point of view, to meet appropriate industrial applications. In fact, a fundamental, systematic and analytical research work is required in this direction.

Hence, in the present work, Taguchi's experimental design technique has been employed to examine the effect and interactions of SMAT parameters on microindentation hardness and surface roughness of AA 6061 aluminum alloy. Further, samples prepared using the optimized condition were characterized with reference to microstructure and nanoindentation hardness measurements.

2. Experimental Procedures

2.1 Material and SMAT Treatment

Al-Mg-Si alloy (AA 6061) was used as the test material. The chemical composition of the material is given in Table 1. Specimens for SMAT treatment were fabricated from AA 6061 available in naturally aged condition (T4). Metallographic polishing was done on the samples first using four different grades of silicon carbide abrasive papers (grit sizes of 400, 600, 800 and 1000) and subsequently using alumina slurry (alumina particles of 1-μm size mixed with water). Final cleaning was done with acetone in an ultrasonic cleaner for 15 min. AA 6061 alloy plate ($120 \times 30 \times 8$ mm^3) was subjected to SMAT using a surface nanocrystallization equipment (model SNC1, Chengdu SNC Advanced Technology Co., Ltd, China). A large number of stainless steel balls (SS 316L) were placed at the bottom of a cylindrical-shaped container that was vibrated by using a vibration generator. As a result, the balls resonated and impacted the surface of the sample kept at the upper portion of the container. The repeated striking of balls at high strain rates led to severe plastic deformation in the entire sample surface. The SMAT was done using stainless steel (AISI 316L) balls of diameter 2, 5 and 8 mm for treatment durations of 15, 30 and 45 min in vacuum (-0.1 MPa) using a vibrating frequency of 50 Hz. The schematic diagram and methodology of SMAT were given elsewhere (Ref 1, 24).

2.2 Material Characterization

X-ray diffraction (XRD) was carried out on the surface of untreated and treated samples using an x-ray diffractometer (Bruker D8 Discover, USA) with Cu Kα radiation. Observations of cross-sectional microstructure and surface morphology were done using a scanning electron microscope (SEM) (FEI Quanta 200, Philips, USA). Surface roughness parameters (R_a and R_{max}) of samples were determined using a surface roughness tester (TR 200, Time Group Inc., China). Vickers microindentation hardness on the surface of the untreated and SMAT samples were measured with a load of 0.2 kg using a microhardness tester (401 MVD, Wolpert Wilson Instruments, USA). A nanoindenter (TI 950 TriboIndenter, Hysitron, USA) was used to measure nanoindentation hardness just below the treated surface at a load of 10 mN. The values of Young's modulus 'E' of the samples were calculated using the following Eq 1.

$$E = \left(1 - v_s^2\right)\left(\frac{1}{E_r} - \frac{\left(1 - v_i^2\right)}{E_i}\right)^{-1} \tag{Eq 1}$$

where v_s is the Poisson's ratio of the sample, E_i is the Young's modulus of the indenter (=1140 GPa), v_i is the Poisson's ratio of the indenter (=0.07), and E_r is reduced modulus.

Microstructural studies were done using a transmission electron microscope (TEM) (CM 12, Philips, USA) operating at 120 kV. Thin foils were prepared for TEM observations using mechanical polishing, electrochemical polishing and ion milling.

2.3 Design of Experiment

Taguchi's experimental design is a powerful technique, which can identify the dominant factors, their influence on the mechanical properties and the interaction between these factors. The choice of the area of experiment and the identification of the suitable process parameters and their levels are based on screening experiments (Ref 25). These process parameters are listed in Table 2. In the present investigation, the influence of two factors, each at three levels, was studied using an L$_9$ (3^2) full-factorial orthogonal design. Two factors, viz., ball diameter (D) and treatment duration (T), were used in this study, and the full-factorial design matrix is shown in Table 3.

3. Results and Discussion

3.1 Surface Roughness

The surface roughness increases significantly after SMAT process, compared to untreated samples ($R_a = 0.25$ μm). A higher value of the surface roughness could mask the positive effects derived from nanostructured surface and compressive residual stress generated by SMAT (Ref 26). It is well established that surface roughness plays a role on the fatigue performance apart from the residual stress. Rough surface profiles can act as potential stress raisers, which increase the local stress, and therefore, crack initiation takes place prematurely in diminishing fatigue performance.

The influence of surface roughness is very complex in the fretting wear process. In case of a smoothly polished surface having a low roughness value, higher friction can be expected

Table 1 Chemical composition (in wt.%) of AA 6061

Element	Mg	Si	Fe	Cu	Mn	Al
Wt.%	0.63	0.55	0.21	0.15	0.30	Balance

Table 2 Factor levels for the experiment

Factors	Level I	Level II	Level III
Ball diameter 'D' (mm)	2	5	8
Treatment duration 'T' (min)	15	30	45

Table 3 Full-factorial design matrix

			Surface roughness		
Sl. no	D, mm	T, min	R_a, µm	R_{max}, µm	Hardness, $H_{V0.2}$
1	2	15	1.410	7.071	74
2	2	30	1.469	7.410	81
3	2	45	1.458	7.057	92
4	5	15	2.787	11.10	95
5	5	30	3.045	11.76	112
6	5	45	2.729	11.09	125
7	8	15	2.894	13.78	96
8	8	30	3.567	15.35	127
9	8	45	3.136	13.00	133

due to higher adhesion and so it leads to higher fretting damage. Also, in this case, the damage may be increased due to the trapped fretting debris at the contact zone acting as abrasive particles causing abrasion damage (Ref 27). On the other hand, in the case of rougher surface, the fretting debris at the contact areas may fall into adjacent valleys, may not act as third-body abrasive particles and reduces the abrasive wear resulting in less fretting damage (Ref 28). Hence, it is very much important to control and understand the development of the surface roughness after the SMAT.

The analysis of influence of SMAT parameters on surface roughness by the experimental design is shown in Fig. 1. It is possible to select appropriate parameters for processing the samples for different testing conditions in Fig. 1(a). For instance, for enhancing fatigue performance or fretting wear resistance of a component, the proper combination of parameters (ball diameter and SMAT duration) resulting in low surface roughness for former and parameters resulting in higher surface roughness for latter could be selected.

Figure 1(b) shows the effect of SMAT parameters on the evolution of roughness R_a. The trend exhibited by R_a value indicates some qualitative similarity for the case of SNH process reported in (Ref 5), i.e., the surface roughness R_a increases sharply at the beginning of treatment and then decreases to achieve a saturation magnitude. However, with bigger balls, the saturation is reached within a shorter period of time compared to that with the smaller balls.

The mean of means of the two factors at each level is shown in Fig. 2(a). It could be seen that the influence of ball diameter on roughness R_a is more predominant than that of the treatment duration. Interaction plots are shown in Fig. 2(b). They help to judge the presence of interaction between parameters. The difference in the response of a parameter at two levels is

(a)

(b)
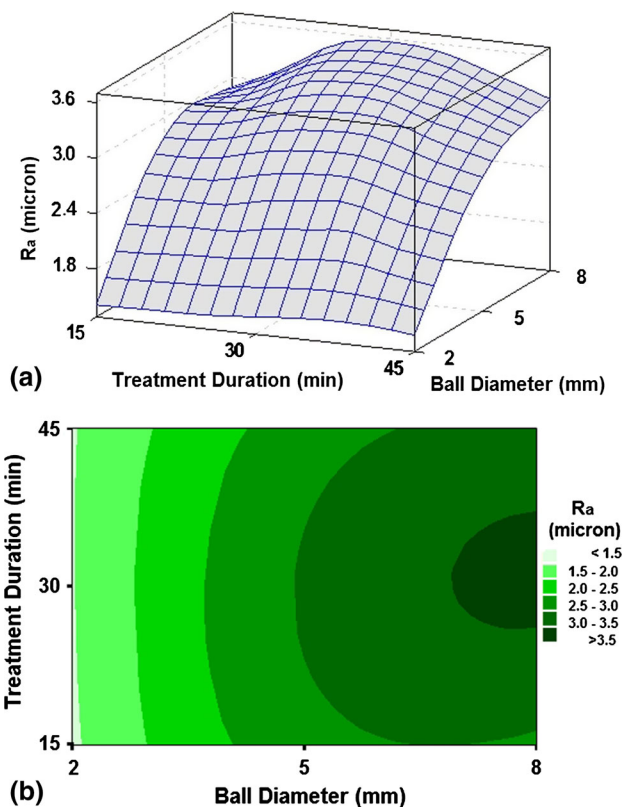
Fig. 1 (a) Variation of roughness R_a; (b) contour of R_a as a function of ball diameter and SMAT duration

dependent on the level of another parameter. If lines in an interactions plot are not parallel, there is interaction. If there is greater deviation from being parallel, the degree of interaction

will be more. It could be seen that the lines are not parallel, which indicates that both treatment duration and ball diameter have a considerable influence on the surface roughness.

Further, the development of surface roughness during the SMAT process found to be dependent on treatment duration. Figure 2(a) shows that the R_a value of the SMAT-treated aluminum sample raises from 0.25 μm in the untreated condition to 2.375 μm during the first 15 min, and with further increase in treatment duration to 30 min, R_a value increases to 2.7 μm. However, R_a value decreases from 2.7 to 2.4 μm with further increase in treatment duration to 45 min. A comparable trend has been observed for 5052 aluminum alloy prepared by SNH process by Dai et al. (Ref 5). They described this trend by assuming the occurrence of the process in three stages. In stage I, the entire surface of the plate is not covered by indents created by the striking balls. A pair of hill and valley is generated by each indent with gaps between two indents. The roughness value monotonously increases with the freshly created indents. During stage II, the plate surface is completely covered by indents without any flat surface. Probably, some

regions would have experienced impacts several times. Also, due to repeated impacts, the hill height continuously decreases, but there is not much change in the valley depth. So the roughness value decreases. In stage III, there is a balance between the rate of generation of hills and valleys and the rate of reduction in hill height. So there is no significant change in the roughness value.

Figure 2(b) shows R_a values of SMAT-treated alloy as a function of the ball diameter. R_a value increases with an increase in ball diameter. Though bigger balls carry greater impact energy during SMAT, at same time the contact area also rises to increase the roughness value. The results are comparable with the reported values by Dai et al. (Ref 5), in which the SNH treatment carried out on aluminum alloy surface with 7.9-mm-diameter balls had higher R_a values compared to that treated with 5-mm-diameter balls.

Mathematical relationships between the surface roughness parameters (R_a or R_{max}) and the studied factors (including their interactions) were established by developing regression equations
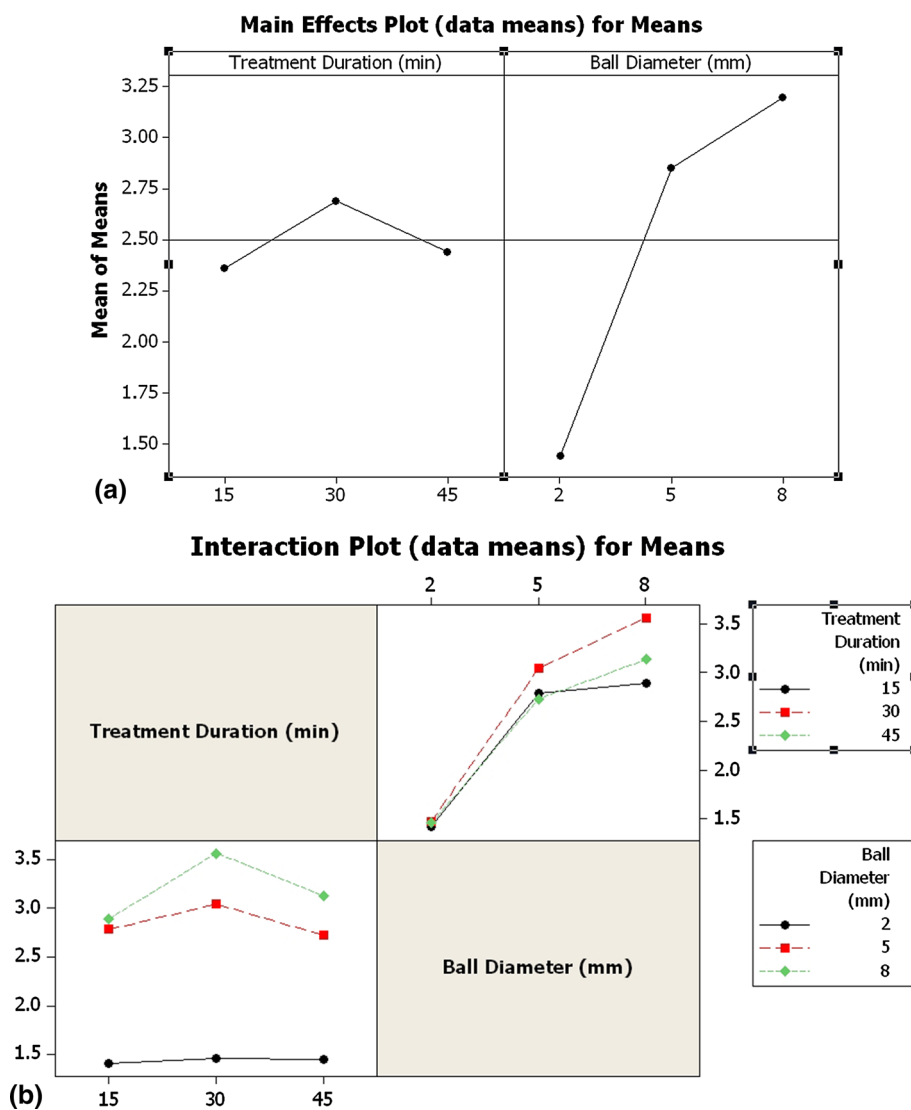

Fig. 2 (a) Main effects of factors on roughness R_a; (b) interaction effect between factors

$$R_a = 0.1516 + 0.2599D + 0.07488T + 0.001078TD$$
$$- 0.00195T^2 \quad (R^2 = 92.1\%) \tag{Eq 2}$$

$$R_{max} = 1.455 + 1.272D + 0.2764T - 0.004256TD$$
$$- 0.004401T^2 \quad (R^2 = 97.3\%) \tag{Eq 3}$$

The regression Eq 2 and 3 may be employed in selecting proper SMAT parameters so that the desired property of the component may be obtained.

Further, analysis of variance (ANOVA) method was used to calculate the significant factor, the so-called Fisher's ratio (F) that affects the surface roughness. The F value for each factor was calculated for surface roughness and is shown in Table 4. The observed F value from F Table (1, 8) for this study is 3.46 at 90% confidence level (Ref 29). Design factors having values of F greater than 3.46 have a significant effect on the surface roughness value. The F value of the ball diameter is 92.21, which is greater than 3.46, and hence, the ball diameter has a significant role on surface roughness. The treatment duration, whose F value is 3.28, which is slightly lower than 3.46, has an insignificant effect on surface roughness based on the 90% level of confidence.

3.2 Hardness

SMAT process increases the surface hardness to a large extent compared to untreated samples (60 H_v), which can be attributed to the significant amount of strain hardening and grain refinement. Both treatment duration and ball diameter have pronounced effect in increasing the surface hardness (Fig. 3). With an increase in the treatment duration, the continuous accumulation of plastic strain will cause significant work hardening. With an increase in ball diameter, the amount of kinetic energy induced to the material surface also increases since kinetic energy is directly proportional to mass of ball. It could be seen that balls with smaller diameter for shorter treatment duration result in lower surface hardness compared to balls with bigger diameter for longer treatment duration. In fact, higher surface hardness is preferred for better fatigue and fretting wear resistance (Ref 27). Figure 3(b) shows the variation of surface hardness as a function of treatment duration and ball diameter. It is evident that SMAT process with bigger ball diameter and longer treatment duration will result in higher surface hardness. Similar findings were reported for SMAT-treated steels (Ref 13). In fact, not only the surface hardness increases, the work-hardened layer thickness also increases by the SMAT treatment duration (see the next section), because of the deeper plastic region and thicker nanocrystalline layer.

The mean of means of the two factors at each level is shown in Fig. 4(a). Both ball diameter and treatment duration have a significant effect on the surface hardness. There was a significant increase in the surface hardness of sample when the ball diameter increased from 2 to 5 mm. However, the increase in surface hardness was not very significant when the ball diameter increased from 5 to 8 mm. Interaction plots are shown in Fig. 4(b). Both treatment duration and ball diameter have a significant influence on the surface hardness as the lines are not parallel.

A mathematical relationship between surface hardness and the studied factors (including their interactions) was established by developing a regression equation

$$H_V = 39.65 + 14.19D + 0.4167T + 0.1056TD$$
$$- 1.13D^2 \quad (R^2 = 96.8\%) \tag{Eq 4}$$

This equation may be used in choosing proper SMAT parameters so as to obtain the desired property of the component.

Further, analysis of variance (ANOVA) method was used to calculate the significant factor, Fisher's ratio (F) that affects the surface hardness. The F (Fisher's ratio) value for each factor was calculated for surface hardness and is shown in Table 5. The observed F value from F Table (1, 8) for this study is 3.46 at 90% confidence level. Design factors having values of F greater than 3.46 have a significant effect on the surface hardness value. The F value for both treatment duration and normal load is greater than 3.46 and so both have a significant role on the surface hardness.
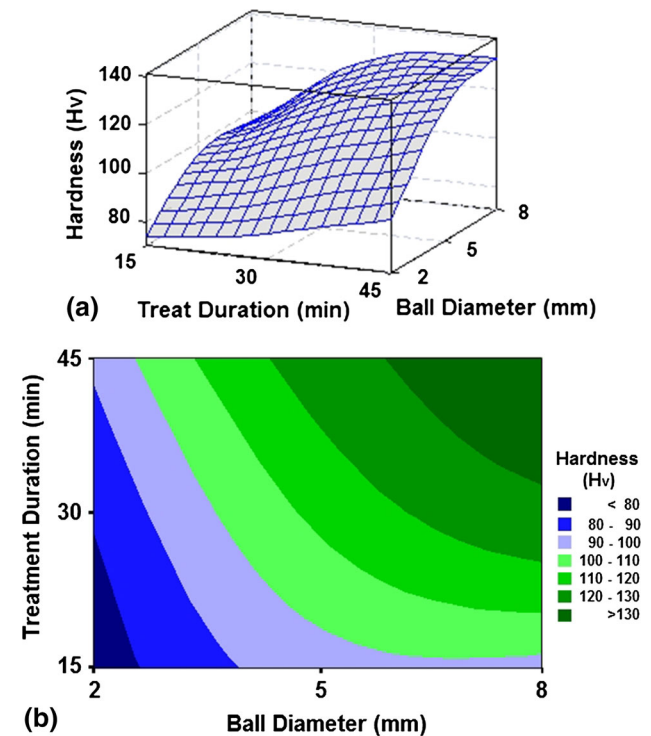

Fig. 3 (a) Variation of surface hardness; (b) contour of surface hardness as a function of ball diameter and SMAT duration

Table 4   Analysis of variance (ANOVA) for surface roughness

Factors	Sum of squares	Degree of freedom	Variance	F value
Treatment duration (min)	0.1787	2	0.089350	3.280
Ball diameter (mm)	5.1759	2	2.587950	92.21
Error	0.1123	4	0.028075	…
Total	5.4669	8	…	…

Main Effects Plot (data means) for Means

(a)
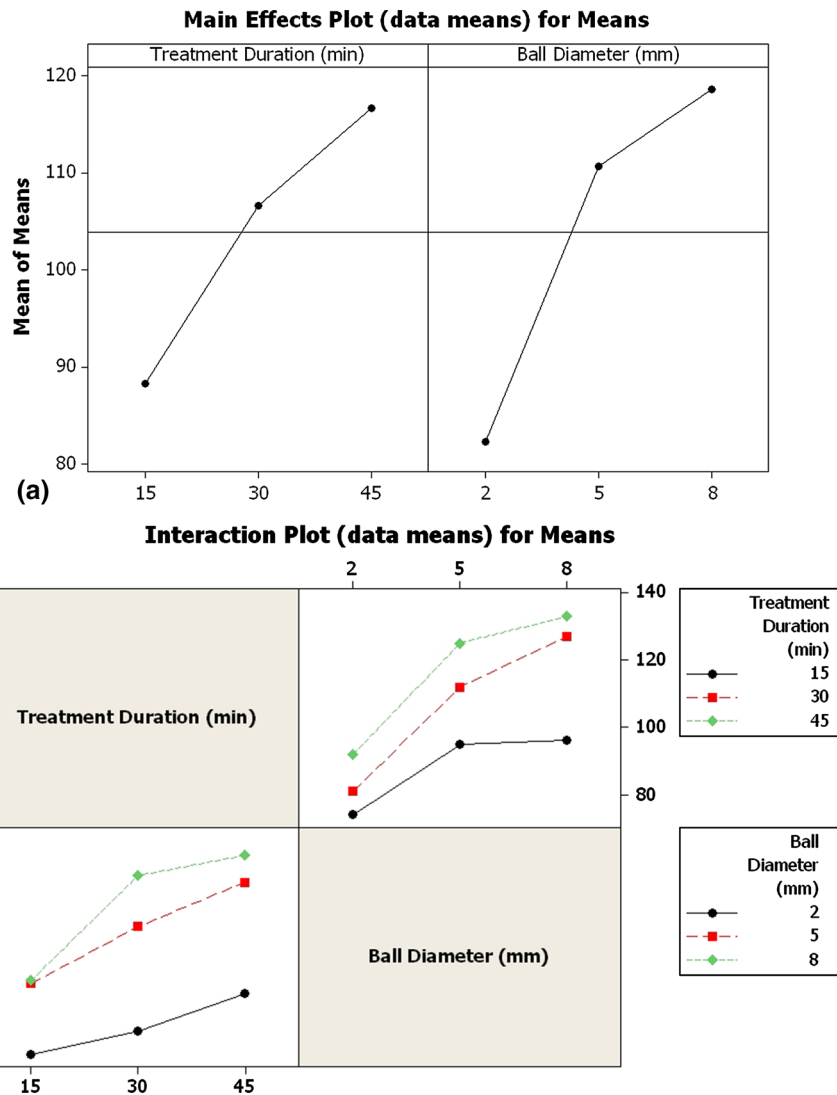
Interaction Plot (data means) for Means

(b)

Fig. 4 (a) Main effects of factors on surface hardness; (b) interaction effect between factors

Table 5 Analysis of variance (ANOVA) for hardness

Factors	Sum of squares	Degree of freedom	Variance	F value
Treatment duration (min)	1238.89	2	619.4450	14.83
Ball diameter (mm)	2186.89	2	1093.445	26.17
Error	167.110	4	41.77750	…
Total	3592.89	8	…	…

In the case of specimens treated with 8-mm-diameter balls, the hardness values are high and the surface roughness value is also very high, which is very detrimental. In addition to that, there was a change in geometry of specimens treated by 8-mm-diameter balls. In the case of samples treated using 2-mm-diameter balls, the surface roughness is low and also the hardness value is less. So the specimens treated with 5-mm-diameter balls for 15 and 45 min were chosen for further characterization studies.

3.3 Characterization

Figure 5 shows the surface morphology of the SMAT-treated sample with 5-mm-diameter balls for two different treatment durations. Depressions or craters may be seen, which were developed by the balls striking the surface during SMAT. In SMAT process, the impact caused by steel balls creates a pileup encasing the crater and generates a new pair of hill and valley on the impacted surface. The topmost point of the pileup and the lowest point of the crater would constitute the hill and valley of the surface, respectively. During SMAT process, the generation of fresh pairs of hill and valley and its magnitude will be greater compared to the initial surface. So, an increment in height of peak to valley would result in R_a values to raise (Ref 5).

Figure 6 shows the cross-sectional views of samples treated for two different durations (15 and 45 min). In the near-surface
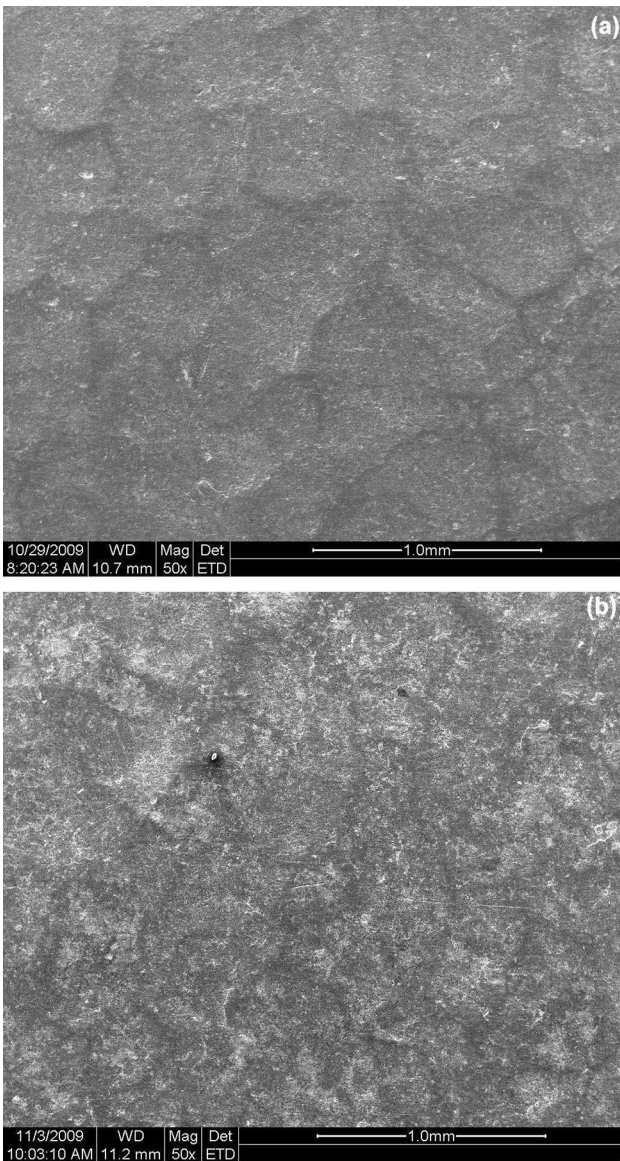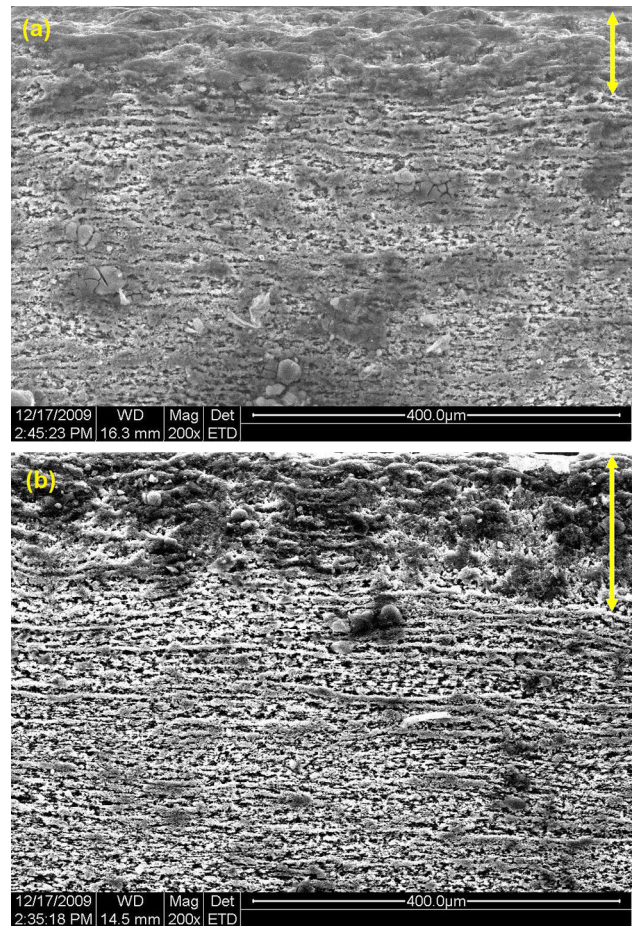
Fig. 5 Surface morphology of SMAT-treated samples with 5-mm-diameter balls for two different treatment durations: (a) 15 min; (b) 45 min
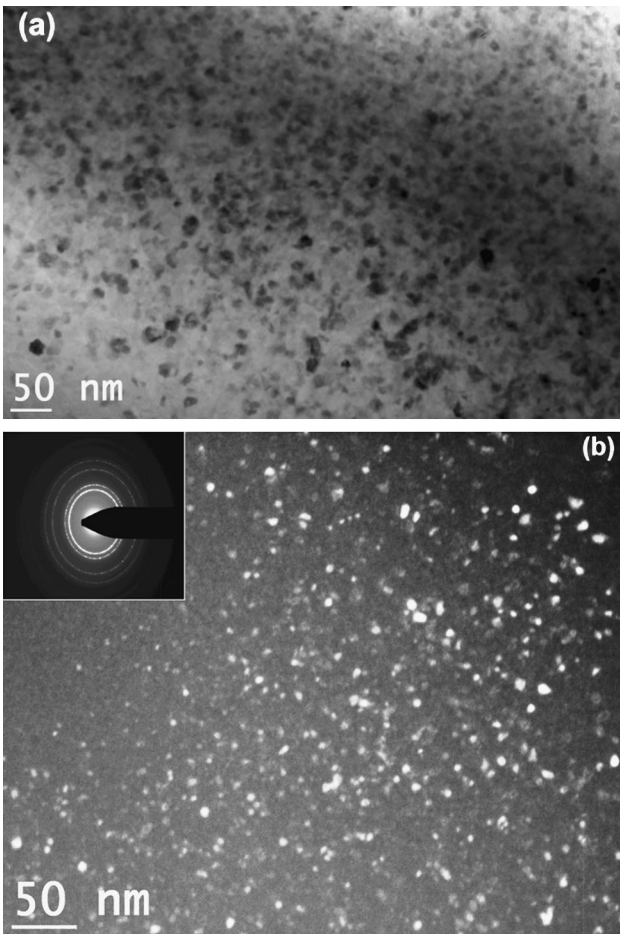

Fig. 6 Cross-sectional views of samples treated with 5-mm-diameter ball for two different durations: (a) 15 min; (b) 45 min. Severe plastic deformed layer is shown by double-headed arrows

layer of SMAT-treated samples, severe plastic deformation could be seen. The depth of severe plastic deformed layer is about 95 and 140 μm for samples treated for 15 and 45 min, respectively. Saitoh et al. (Ref 30) reported the formation of finer grains near the surface of alloy steel sample subjected to air blast shot peening. They suggested that the coarse grains were progressively refined to very fine grains in the near-surface regions, due to severe plastic deformation introduced by steel balls striking at high strain rates.

SMAT process induced a grain size gradient microstructure (finer grains in the surface and undeformed coarse grains at the bulk of the material) across the cross section. It is well established that fatigue properties of metallic materials are strongly influenced by both grain size and residual stresses. Nanostructured grains could significantly increase the yield strength to improve the fatigue crack initiation resistance in the materials. But such finer grain size has a detrimental effect on the fatigue crack propagation resistance, due to poor ductility
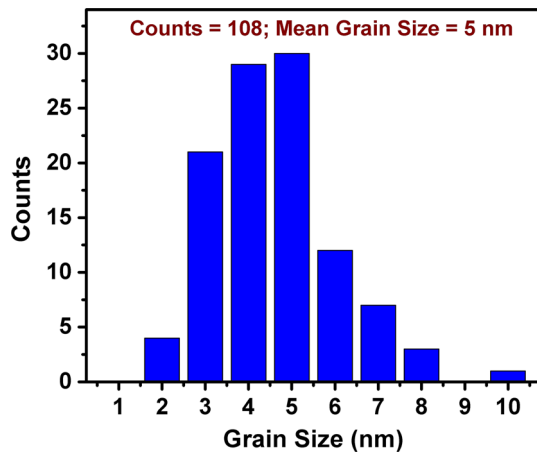
and toughness of the materials. Coarse-grained metallic materials are not capable of avoiding or delaying the initiation of the fatigue crack due to lower tensile strength (Ref 31). However, they may exhibit superior crack propagation resistance due to good ductility and toughness. In view of the fact that the fatigue cracks develop from the surface and subsequently propagate to the interior, so a component with a nanostructured layer at the surface and coarse-grained interior could be anticipated to have superior fatigue lives.

Figure 7 shows the bright-field and dark-field TEM images of top surface layer of a specimen treated with 5-mm-diameter balls for 45 min. SMAT resulted in the formation of nanocrystalline structure on the surface of samples. The selected area electron diffraction (SAED) pattern confirms the formation of nanocrystalline grains on the treated surface. Grain size distribution at the top surface layer determined from the TEM images is given in Fig. 8. It may be seen that the mean grain size is found to be 5 nm ± 1 nm. Figure 9 shows the dark-field TEM image of top surface layer of a specimen treated with 5-mm-diameter balls for 15 min. Grain size distribution at the top surface layer determined from the TEM image is given in Fig. 10. The mean grain size is found to be 11 nm ± 1 nm. It may be noted that with an increase in the treatment duration from 15 to 45 min, the average grain size reduced from 11 to 5 nm.

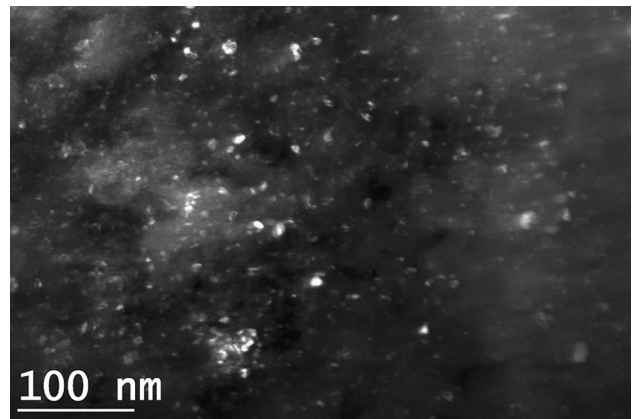Fig. 9 Dark-field TEM image of the surface layer of a sample treated with 5-mm-diameter balls for 15 min

Fig. 7 (a) Bright-field, (b) dark-field TEM images and corresponding SAED pattern of the surface layer of a sample treated with 5-mm-diameter balls for 45 min
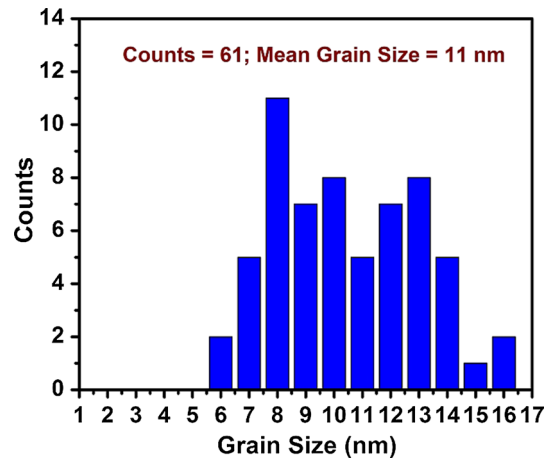

Fig. 10 Grain size distribution on the SMAT-treated surface of a sample treated with 5-mm-diameter balls for 15 min

Fig. 8 Grain size distribution on the SMAT-treated surface of a sample treated with 5-mm-diameter balls for 45 min

The crystal structure of the material and the imposed deformation conditions are the important factors, which strongly influence the grain refinement. Slip and twinning are responsible for the plastic deformation of metallic materials. Slip is the dominant mechanism in metallic materials having medium or high stacking fault energy (SFE), and twinning is favorable in metals having low SFE, especially at high strain rates and/or at low deformation temperatures.

Based on systematic high-resolution transmission electron microscopic observations, Wu et al. (Ref 7) had described the mechanism of the development of nanostructured surface for USSP-treated aluminum alloy 7075. Nanocrystallization in aluminum alloy 7075 takes place through the formation of dislocation cells inside the coarse grains, and subsequently, these cells are separated by dislocation dense walls (DDWs) and dislocation tangles (DTs). Due to accumulation of very large plastic strain, the dislocation cells are transformed into subgrains via subgrain rotation. At the same time, formation of finer dislocation cells separated by DDWs and DTs continues in other coarse grains as well as in subgrains. Nanometer-sized equiaxed grains in random orientations develop due to high density of dislocation cells inside the subgrains.

It may be noted that aluminum alloy 6061 used in the present work is similar to aluminum alloy 7075. The value of SFE of aluminum alloy 6061 is 150 mJ/m^2 (Ref 32), which is closer to that of aluminum alloy 7075, i.e., 125 mJ/m^2 (Ref 33). It is suggested that a similar mechanism might be responsible for nanocrystallization in aluminum alloy 6061 also. However,
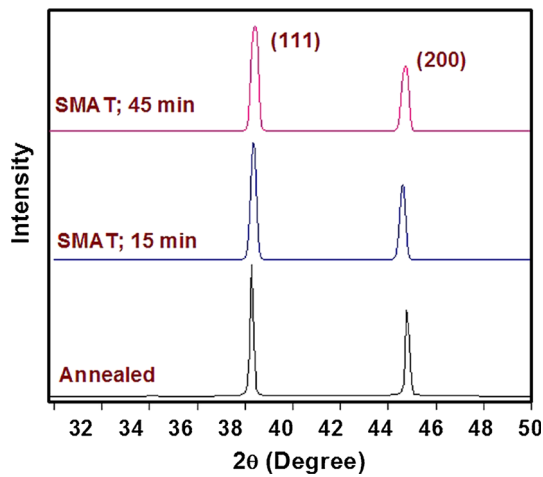
Fig. 11 XRD patterns of an annealed sample and SMAT-treated samples with 5-mm-diameter ball for two different durations

Table 6 Average crystallite size of the surface of the SMAT-treated samples by XRD method

| Sample condition	Average grain size, nm
SMAT, 5 mm dia, 15 min	66
SMAT, 5 mm dia, 45 min	45

this should be confirmed by detailed electron microscopic observations.

The XRD patterns of samples in the annealed condition and treated conditions are shown in Fig. 11. In case of samples treated by SMAT, the Bragg diffraction peaks show broadening and this is attributed to the reduction in crystallite size. The average crystallite sizes, calculated from the broadening of (111) and (200) Bragg diffraction profiles using Debye-Scherrer relation (Ref 34), are shown in Table 6. It is noticed that an increase in the treatment duration resulted in the reduction in the average crystallite size.

Further, the crystallite size from the transmission electron micrograph was found to be smaller compared with the XRD observations (Table 6). It may be noted that the foils for transmission electron microscopy were prepared from the top surface layer (SMAT-treated surface) with the thickness not exceeding 5 μm. On the other hand, the penetration depth of x-rays in aluminum material is about 60 μm (Ref 35), and therefore, XRD results average the information of SMAT-treated surface layer of 60 μm thickness. Also, the grain size increases with an increase in the plastically deformed depth. As a result, the average crystallite size determined by XRD is found to be higher compared to the grain size observed from TEM images.

3.4 Nanoindentation Hardness

The influence of SMAT duration on the near-surface hardness and load-displacement plots is shown in Fig. 12. The hardness decreases with the distance from the SMAT-treated surface due to severe plastic deformation at and near the treated surface. Higher hardness is noticed in the sample treated for a longer duration. This is due to the presence of finer grain size and strain hardening with an increase in treatment duration. Beyond 50 μm depth from the surface, the SMAT duration did
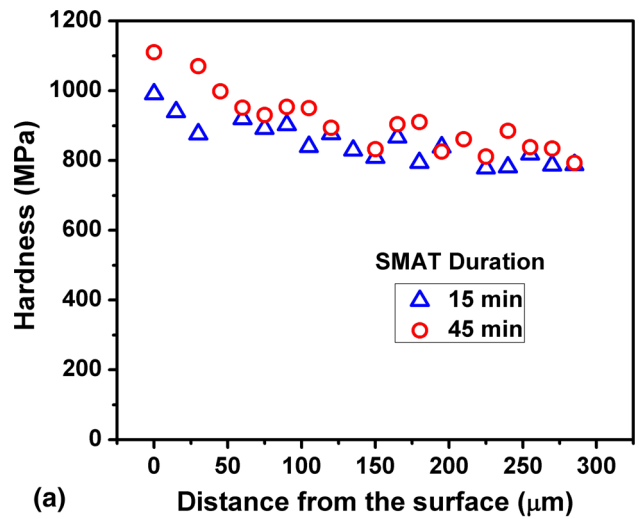
(a)
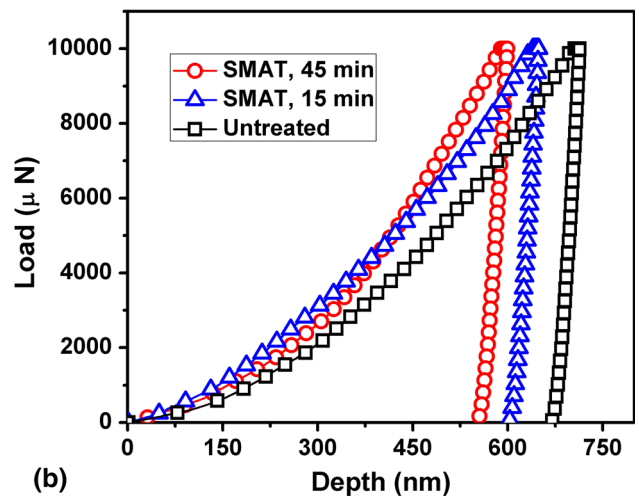
(b)

Fig. 12 (a) Variation of nanoindentation hardness with distance from surface of samples treated with 5-mm-diameter balls; (b) typical load-displacement curves of untreated and SMAT-treated samples

not result in a significant difference in hardness value (Fig. 12a). A similar trend of decreasing hardness with the distance from the SMAT-treated surface has been reported by other researchers (Ref 8, 11).

Figure 12(b) shows the typical nanoindentation load-displacement curves of samples in different conditions before and after SMAT. Considering the area formed by loading and unloading load-displacement (depth) curves, it may be noted that the sample treated for 45 min shows smaller area compared to the sample treated for 15 min (Fig. 12b). This area is taken as plastic deformation work, and this can be used to evaluate the resistance to plastic deformation and the wear resistance (Ref 36). So the sample treated for longer durations exhibits smaller plastic deformation work. In case of SMAT-treated samples for 45 and 15 min and untreated sample subjected to the same load of 10 mN, the indenter penetrated to a depth of 599, 649 and 714 nm, respectively. The relatively lower depth of penetration in SMAT-treated samples may be attributed to the introduction of compressive residual stress in the surface layer by SMAT process. Zhu et al. (Ref 37) explained the influence of nature of residual stresses on the load-depth curve obtained by nanoindentation technique for the same value of

maximum depth in case of (100) copper single crystal. They observed lesser load for tensile residual-stressed sample and higher load for compressive residual-stressed sample compared to unstressed sample for the same value of maximum depth. As the indentation stress acts normal to the sample surface, the direction of contact shear stress underneath the indenter is the same with the tensile residual stress direction. Hence, the tensile residual stress enhanced the amount of shear stress relatively to the unstressed samples. The magnitude of shear stress in case of tensile residual-stressed sample can increase the plastic deformation due to indentation. Hence, lesser load was required compared to the unstressed state for the same indentation depth. The converse was true regarding the influence of compressive stress state. They reported that the nature of residual stress had a significant impact on the shapes of the loading curves. The loading curve for compressive stress had higher slope and shifted leftward compared to unstressed state. On other hand, in the case of tensile stress, the loading curve had a lower slope and shifted right side compared to unstressed state. In the present study, lower penetration depth of 599 and 649 nm corresponds to SMAT-treated sample for 45 and 15 min, respectively, and their loading curves are toward left side of the untreated (unstressed) sample's loading curve. From this, it may be said that SMAT process induced compressive residual stress in the surface layers of 6061 aluminum alloy.

It is well established that the presence of compressive residual stresses increases the elastic modulus value (Ref 38). The values of elastic modulus were calculated using Eq 1, and they were found to be 84, 79 and 73 GPa for SMAT-treated samples for 45 min, SMAT-treated samples for 15 min and untreated samples, respectively. From these values, it may be assumed that SMAT-treated sample for 45 min had higher magnitude of compressive residual stress compared to SMAT-treated sample for 15 min. However, it needs experimental verification.

4. Conclusions

Based on the results obtained in the present study on the influence of surface mechanical attrition treatment (SMAT) parameters (ball diameter and treatment duration) on the microstructural and mechanical properties of AA 6061, the following conclusions are drawn. Due to SMAT, nanocrystallites formed on the surface and near-surface regions. The average crystallite size decreased with an increase in treatment duration. SMAT process induced a grain size gradient microstructure (finer grains in the surface and undeformed coarse grains at the bulk of the material) across the cross section. The depth of severe plastic deformed layer increased with an increase in treatment duration. The surface roughness increased significantly after SMAT process, compared to untreated samples. Balls with smaller diameter for shorter treatment duration resulted in lower surface hardness compared to balls with bigger diameter for longer treatment duration. The ball diameter was the most influencing SMAT parameter compared to the treatment duration. However, interaction between ball diameter and treatment duration could not be ignored. The Taguchi's experimental design technique together with developed regression equations could serve as a guideline for manufacturing industries in relating the SMAT parameters

to the surface properties. The ball diameter and treatment duration could thus be properly selected in SMAT process as per the required values of roughness and/or hardness in order to meet the demand of engineering applications involving fatigue and fretting wear loadings.

References

1. K. Lu and J. Lu, Nanostructured Surface Layer on Metallic Materials Induced by Surface Mechanical Attrition Treatment, *Mater. Sci. Eng., A*, 2004, **375**, p 38–45

2. H. Gleiter, Nanostructured Materials: Basic Concepts and Microstructure, *Acta Mater.*, 2000, **48**, p 1–29

3. K.S. Kumar, H. Van Swygenhoven, and S. Suresh, Mechanical Behavior of Nanocrystalline Metals and Alloys, *Acta Mater.*, 2003, **51**, p 5743–5774

4. J.L. Liu, M. Umemoto, Y. Todaka, and K. Tsuchiya, Formation of a Nanocrystalline Surface Layer on Steels by Air Blast Shot Peening, *J. Mater. Sci.*, 2007, **42**, p 7716–7720

5. K. Dai, J. Villegas, Z. Stone, and L. Shaw, Finite Element Modeling of the Surface Roughness of 5052 Al Alloy Subjected to a Surface Severe Plastic Deformation Process, *Acta Mater.*, 2004, **52**, p 5771–5782

6. G. Liu, J. Lu, and K. Lu, Surface Nanocrystallization of 316L Stainless Steel Induced by Ultrasonic Shot Peening, *Mater. Sci. Eng., A*, 2000, **286**, p 91–95

7. X. Wu, N. Tao, Y. Hong, B. Xu, J. Lu, and K. Lu, Microstructure and Evolution of Mechanically-Induced Ultrafine Grain in Surface Layer of Al-Alloy Subjected to USSP, *Acta Mater.*, 2002, **50**, p 2075–2084

8. H.W. Chang, P.M. Kelly, Y.N. Shi, and M.X. Zhang, Effect of Eutectic Si on Surface Nanocrystallization of Al–Si Alloys by Surface Mechanical Attrition Treatment, *Mater. Sci. Eng., A*, 2011, **530**, p 304–314

9. H.W. Chang, P.M. Kelly, Y.-N. Shi, and M.-X. Zhang, Thermal Stability of Nanocrystallized Surface Produced by Surface Mechanical Attrition Treatment in Aluminum Alloys, *Surf. Coat. Technol.*, 2012, **206**, p 3970–3980

10. Y. Liu, B. Jin, and J. Lu, Mechanical Properties and Thermal Stability of Nanocrystallized Pure Aluminum Produced by Surface Mechanical Attrition Treatment, *Mater. Sci. Eng., A*, 2015, **636**, p 446–451

11. L. Wen, Y. Wang, Y. Zhou, L. Guo, and J. Ouyang, Iron-Rich Layer Introduced by SMAT and Its Effect on Corrosion Resistance and Wear Behavior of 2024 Al Alloy, *Mater. Chem. Phys.*, 2011, **126**, p 301–309

12. L. Wen, Y. Wang, Y. Zhou, L. Guo, and J. Ouyang, Microstructure and Corrosion Resistance of Modified 2024 Al Alloy Using Surface Mechanical Attrition Treatment Combined with Microarc Oxidation Process, *Corros. Sci.*, 2011, **53**, p 473–480

13. B. Arifvianto, Suyitno, M. Mahardika, P. Dewo, P.T. Iswanto, and U.A. Salim, Effect of Surface Mechanical Attrition Treatment (SMAT) on Microhardness, Surface Roughness and Wettability of AISI 316L, *Mater. Chem. Phys.*, 2011, **125**, p 418–426

14. T. Roland, D. Retraint, K. Lu, and J. Lu, Fatigue Life Improvement Through Surface Nanostructuring of Stainless Steel by Means of Surface Mechanical Attrition Treatment, *Scr. Mater.*, 2006, **54**, p 1949–1954

15. N.R. Tao, M.L. Sui, J. Lu, and K. Lu, Surface Nanocrystallization of Iron Induced by Ultrasonic Shot Peening, *Nano Mater.*, 1999, **11**, p 433–440

16. X. Yong, G. Liu, and K. Lu, Characterization and Properties of Nanostructured Surface Layer in a Low Carbon Steel Subjected to Surface Mechanical Attrition, *J. Mater. Sci. Technol.*, 2003, **19**, p 1–4

17. K.Y. Zhu, A. Vassel, F. Brisset, K. Lu, and J. Lu, Nanostructure Formation Mechanism of α-Titanium Using SMAT, *Acta Mater.*, 2004, **52**, p 4101–4110

18. Y.S. Zhang and Z. Han, Fretting Wear Behavior of Nanocrystalline Surface Layer of Pure Copper Under Oil Lubrication, *Tribol. Lett.*, 2007, **27**, p 53–59

19. S. Anand Kumar, S. Ganesh Sundara Raman, T.S.N. Sankara Narayanan, and R. Gnanamoorthy, Influence of Surface Mechanical Attrition Treatment on Fretting Wear Behavior of Ti-6Al-4V, *Adv. Mater. Res.*, 2012, **463–464**, p 316–320

20. S. Anand Kumar, S. Ganesh Sundara Raman, T.S.N. Sankara Narayanan, and R. Gnanamoorthy, Fretting Wear Behaviour of Surface Mechanical Attrition Treated Alloy 718, *Surf. Coat. Technol.*, 2012, **206**, p 4425–4432

21. Y.S. Zhang, K. Wang, Z. Han, and G. Liu, Dry Sliding Wear Behavior of Copper with Nano-scaled Twins, *Wear*, 2007, **262**, p 1463–1470

22. S. Anand Kumar, S. Ganesh Sundara Raman, and T.S.N. Sankara Narayanan, Influence of Surface Mechanical Attrition Treatment Duration on Fatigue Lives of Ti-6Al-4V, *Trans. Indian Inst. Met.*, 2014, **67**(1), p 137–141

23. S. Anand Kumar, S. Ganesh Sundara Raman, and T.S.N. Sankara Narayanan, Effect of Surface Mechanical Attrition Treatment on Fatigue Lives of Alloy 718, *Trans. Indian Inst. Met.*, 2012, **65**, p 473–477

24. T. Balusamy, S. Kumar, and T.S.N. Sankara Narayanan, Effect of Surface Nanocrystallization on the Corrosion Behavior of AISI, 409 Stainless Steel, *Corros. Sci.*, 2010, **52**, p 3826–3834

25. P.J. Ross, *Taguchi Techniques for Quality Engineering*, McGraw-Hill, New York, 1996

26. L. Wagner, Mechanical Surface Treatments on Titanium, Aluminum and Magnesium Alloys, *Mater. Sci. Eng., A*, 1999, **263**, p 210–216

27. Y. Fu, J. Wei, and A.W. Batchelor, Some Considerations on the Mitigation of Fretting Damage by the Application of Surface-Modification Technologies, *J. Mater. Process. Technol.*, 2000, **99**, p 231–245

28. C. Colombie, Y. Berthier, A. Floquet, L. Vincent, and M. Godet, Fretting Load-Carrying Capacity of Wear Debris, *ASME J. Tribol.*, 1984, **106**, p 185–194

29. R.K. Roy, *A Primer on Taguchi Method*, Van Noshtrand Reinhold Int. Co. Ltd, New York, 1990

30. H. Saitoh, T. Ochi, M. Kubota, Formation of surface nanocrystalline structure in steels by air blast shot peening, in *Proceedings of the 10th International Conference on Shot Peening*, (2008), p. 488–493

31. B.N. Mordyuk and G.I. Prokopenko, Ultrasonic Impact Peening for the Surface Properties' Management, *J. Sound Vib.*, 2007, **308**, p 855–866

32. V.S. Sarma, J. Wang, W.W. Jian, A. Kauffmann, H. Conrad, J. Freudenberger, and Y.T. Zhu, Role of Stacking Fault Energy in Strengthening Due to Cryo-Deformation of FCC Metals, *Mater. Sci. Eng., A*, 2010, **527**, p 7624–7630

33. D.E. Stegall, M.A. Mamun, and A.A. Elmustafa, The Role of Stacking Fault Energy on the Indentation Size Effect of FCC Pure Metals and Alloys, *Mater. Res. Soc. Symp. Proc.*, 2012, **1424**, p 7–12

34. B.D. Cullity, *Elements of x-ray Diffraction*, Addison Wesley, Massachusetts, 1978

35. H. Chen, Y.L. Yao, J.W. Kysar, I.C. Noyan, and Y. Wang, Fourier Analysis of x-ray Micro-diffraction Profiles to Characterize Laser Shock Peened Metals, *Int. J. Solids Struct.*, 2005, **42**, p 3471–3485

36. S. Anand Kumar, R. Sundar, S. Ganesh Sundara Raman, H. Kumar, R. Gnanamoorthy, R. Kaul, K. Ranganathan, S.M. Oak, and L.M. Kukreja, Fretting Wear Behavior of Laser Peened Ti-6Al-4V, *Tribol. Trans.*, 2012, **55**, p 615–623

37. L. Zhu, B. Xu, H. Wang, and C. Wang, Effect of Residual Stress on the Nanoindentation Response of (100) Copper Single Crystal, *Mater. Chem. Phys.*, 2012, **136**, p 561–565

38. A.C. Fischer-Cripps, *Nanoindentation*, Springer, New York, 2011